Journal of Cleaner Production 251 (2020) 119710

Contents lists available at ScienceDirect

Journal of Cleaner Production

journal homepage: www.elsevier.com/locate/jclepro

Power consumption estimation for mask image projection stereolithography additive manufacturing using machine learning based approach

Yiran Yang [a], Miao He [b], Lin Li [b, *]

[a] Department of Industrial, Manufacturing, & Systems Engineering, University of Texas at Arlington, Arlington, TX, 76010, USA
[b] Department of Mechanical and Industrial Engineering, University of Illinois at Chicago, Chicago, IL, 60607, USA

ARTICLE INFO

Article history:
Received 11 November 2018
Received in revised form
5 November 2019
Accepted 12 December 2019
Available online 13 December 2019

Handling Editor: Prof. Jiri Jaromir Klemeš

Keywords:
Additive manufacturing
Mask image projection stereolithography
Power consumption
Geometry characteristics
Machine learning

ABSTRACT

Additive manufacturing (AM) or 3D printing has been implemented in a wide range of areas, owing to its superior capabilities of fabricating complex geometries with high design freedom compared to traditional manufacturing. In recent years, the potential environmental impacts that can be caused by AM processes and materials have attracted increasing attentions. Research efforts have been conducted to study and attempt to enhance the environmental performance of AM. In current literature on AM energy consumption, most studies focus on the production stage and investigate the relation between energy consumption and process parameters (i.e., layer thickness). In this work, multiple geometry characteristics (e.g., surface areas and shapes) at each printing layer are studied and linked with the power consumption of mask image projection stereolithography using machine learning based approach. The established models will be able to provide AM designers with a useful tool for estimating power consumption based on layer-wise geometry information in the design stage and promote the awareness of cleaner production in AM. In this work, effective features are selected and/or extracted from layer-wise geometry characteristics and used to train and test machine learning models. According to our results, the shallow neural network has the lowest averaged root-mean-square error (RMSE) of 0.75% considering both training and testing, and the stacked autoencoders (SAE) structure has the best testing performance with RMSE of 0.85%.

1. Introduction

Additive manufacturing (AM) is defined as "the process of joining materials to make objects from 3D model data, usually layer upon layer, as opposed to subtractive manufacturing methodologies" (ASTM, 2012). Owing to the unique layer-wise fabrication method, AM technologies have great advantages including enhanced manufacturing complexity, reduced production time, less material waste, and higher level of customization and design freedom. As a result, the global AM market was estimated to have exceeded $7.3 million U.S. dollars in 2017 (Wohlers Report, 2018), and it will reach an economic impact of up to $550 billion per year in 2020 (Manyika et al., 2013). Nevertheless, limitations and challenges still exist in AM and hinder the large-scale application of AM. For example, the print quality is not consistently satisfactory, and increasing concerns have been presented regarding the potential environmental consequences that can be caused by AM processes/materials.

In current literature, numerous research efforts have been conducted to address the limitations in AM. For example, new technologies/processes have been developed (Li et al., 2018a; Lu et al., 2017), the dimensional accuracy and surface quality of AM fabricated parts have been studied (Dambatta and Sarhan, 2016; Li et al., 2018b), the key cost drivers have been identified (Lindemann et al., 2012; Yang and Li, 2018a), and the mechanical properties of AM printed products have been investigated (Choren et al., 2013; Domingo-Espin et al., 2015; Yang et al., 2019). In particular, the environmental sustainability aspects of AM have been explored including energy consumption (Balogun et al., 2014; Baumers et al., 2011; Meteyer et al., 2014; Paul and Anand, 2012; Sreenivasan and Bourell, 2009; Telenko and Conner Seepersad, 2012; Telenko and Seepersad, 2010; Verma and Rai, 2013; Xu et al., 2015; Yang et al.,

* Corresponding author.
E-mail address: linli@uic.edu (L. Li).

https://doi.org/10.1016/j.jclepro.2019.119710
0959-6526/

Notation list

$\mathbf{I}$	The vector contains a set of geometry-related indexes
$\mathbf{P}$	The vector contains the sensitive subset of geometry-related indexes
$\mathbf{T}$	The principal component space
$\mathbf{T_c}$	The critical principal component space
$\mathbf{P_{PCC}}$	The vector of sensitive indexes selected by Pearson correlation coefficient
$\mathbf{P_{LC}}$	The vector of sensitive indexes selected by Laplacian Score
$\mathbf{U}$	The left singular vectors of index vector $\mathbf{I}$
$\mathbf{\Sigma}$	The rectangular diagonal matrix of square root of the eigenvalues of $\mathbf{I^T I}$ as singular values
$\mathbf{W}$	The right singular vectors of index vector $\mathbf{I}$
$\mathbf{I_N}$	The normalized vector $\mathbf{I}$

2017), process emissions (Afshar-Mohajer et al., 2015; Timothy et al., 2017; Yang and Li, 2018b), and material use/waste (Meteyer et al., 2014).

These existing studies on AM environmental sustainability have facilitated the understandings on the energy and material flows in different AM processes. The results of these studies are beneficial for AM production planning and optimization towards environmental sustainability, e.g., selecting appropriate process parameters like layer thickness. In fact, adjusting the geometry designs can also contribute to improved environmental performance especially reduced power consumption. In current literature, research efforts have been conducted to link the geometry design with power consumption, but they mainly focus on part positioning and orientation (Balogun et al., 2015; Baumers et al., 2012; Verma and Rai, 2013; Yang et al., 2017). For example, several different part printing positions and orientations are investigated for their effects on energy consumption (Mognol et al., 2006). As another example, Yang et al. (2017) found out that certain part position angle can lead to reduced energy consumption using design of experiment method. While these studies can provide useful insights on selecting and optimizing the part orientations and positions, they did not consider how layer-wise geometry characteristics (i.e., surface area of a certain layer) can affect the power consumption, which is critical especially in processes like mask image projection (MIP) stereolithography (SL). Such relation between power consumption and layer-wise geometry characteristics has not yet been well studied, and it will be able to greatly aid AM designers to consider potential power consumption when they generate and optimize the geometry designs.

To fill the above-mentioned research gap, this work aims to characterize the relation between layer-wise geometry characteristics and energy consumption of MIP SL process using machine learning based approaches. The main reasons for adopting data-driven method are the easy access to power monitoring data in typical industrial settings and the ability of data-driven models in terms of predicting the energy consumption without requiring comprehensive knowledge on the process mechanisms. To obtain the most effective predictors from layer-wise geometry characteristics (mainly concerned with surface areas and shapes), three methods are used, i.e., feature selection by sensitivity analysis, manual feature extraction using principal component analysis (PCA), and automatic feature extraction using stacked autoencoders (SAE). These selected/extracted features are then used for training and testing three models, i.e., regression, neural network, and deep learning-based model. The machine learning based models established in this work can enable a prior prediction on power consumption for a certain geometry design, and hence can aid AM designers to adjust or even optimize geometry designs for cleaner production.

The rest of this paper is organized as follows. In Section 2, methodologies used for feature selection/extraction are introduced. In Section 3, the results are presented including the model performance of trained machine learning models, a sensitivity analysis and discussions. Finally, in Section 4, conclusions and future work are discussed.

2. Methodologies

The proposed framework for obtaining the most effective geometry-related features to estimate and predict the energy consumption is illustrated in Fig. 1. A set of layer-wise geometry-related indexes are selected as potential attributes for estimating the energy consumption. Based on these geometry-related indexes, features are obtained using three approaches: (1) feature selection based on sensitivity analysis using Pearson correlation coefficient and Laplacian Score; (2) manual feature extraction based on PCA results; and (3) automatic feature extraction through SAE. Based on the selected/extracted features, three machine learning-based prediction models (i.e., linear regression model, neural network model, and deep learning-based model) are trained and compared for their performance on power consumption estimation. Note that, as shown in Fig. 1, the selected sensitive geometry indexes and critical components are used in linear regression and neural network models for comparison, and the complete set of geometry indexes are used for automatic feature extraction in deep learning structure.

2.1. The stereolithography process illustration and data collection

The MIP SL process studied in this work is illustrated in Fig. 2(a). The production process starts with the first layer image being projected to the build platform and solidified by the Ultraviolet (UV) light. Once the first layer is finished, the build platform moves vertically up for the distance of a layer thickness for the next layer printing. This procedure is repeated until the entire part is fabricated. During the production, several energy consumers exist, i.e., the projector, the build platform movement, and the control

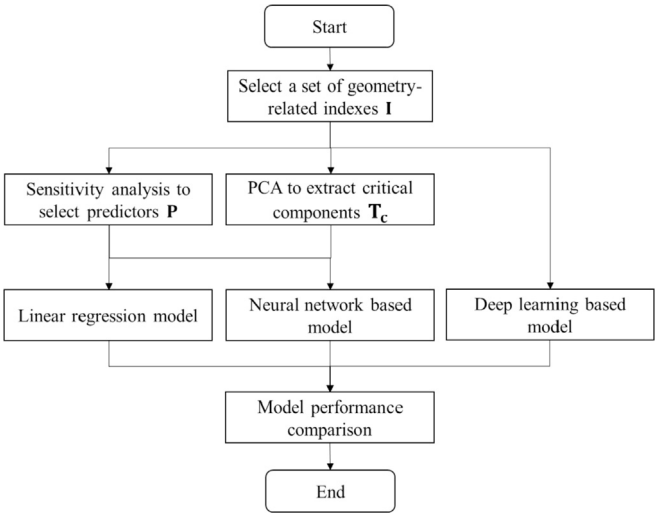

Fig. 1. The flow chart of proposed framework.

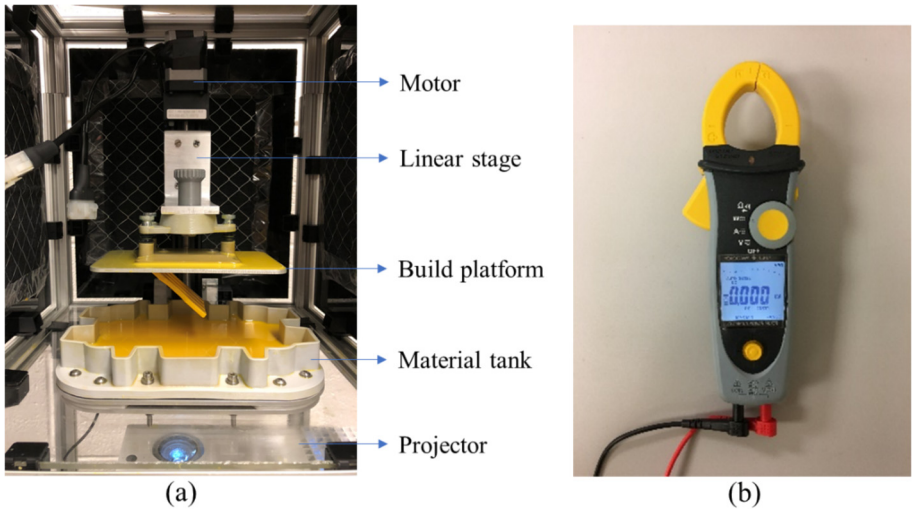

Fig. 2. Illustrations of (a) the mask image projection stereolithography process, and (b) the power meter for data collection.

system. In this work, the energy consumption from the projector and the build platform is considered. It should be noted that this study is limited in the actual 3D printing process excluding the preprocessing (or design) and postprocessing stages (cleaning).

The power consumption is measured using a clamp-on power meter CW10 by Yokogawa as shown in Fig. 2(b). This power meter is clamped on the wires of studied electricity consumer. Note that the power data is recorded with a 2-second time interval. This power meter can monitor up to 600 kW with 1000V maximum AC/DC voltage and 600A maximum AC/DC current. The power data is collected during the printing of geometries shown in Fig. 3. The total number of sampled power data is 657, where 311 is from the fabrication of geometry No.1, and 346 is from the fabrication of geometry No.2. In addition, 60% of the sampled data (394) is used for model training, and 40% of the sampled data (263) is used for model testing. In particular, 70%, 15% and 15% of training dataset is randomly sampled for training, validating and testing at the training stage of neural network and SAE, respectively. It should be noted that layer-wise geometry characteristics are used in further analysis rather than the entire 3D model of geometry No.1 and No.2.

2.2. Index selection and sensitivity analysis

By using the MIP SL process for part fabrication, each layer is solidified by the UV light, which, subsequently, implies that layer-wise geometry characteristics would have impact on the energy consumption required for each layer. In this work, a set of geometry-related indexes **I** is selected as attributes, i.e., area-related and curvature-related indexes. More specifically, area-related characteristics are used to investigate impact of the surface areas on the required power consumption; and curvature-related indexes are selected to represent the complexity of each layer image. It should be noted that curvature cannot be used as the sole criteria when evaluating the complexity.

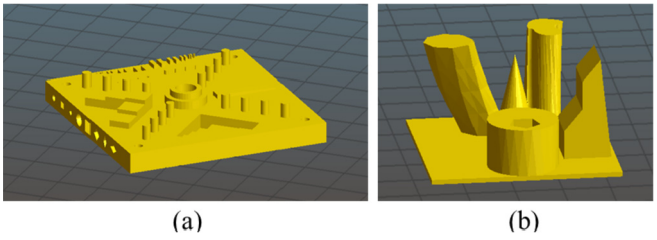

Fig. 3. The 3D geometries printed for data collection: (a) part No.1 and (b) part No.2.

To identify a sensitive subset of geometry-related indexes **P** as predictors, sensitivity analysis is performed. Note that $\mathbf{P} \in \mathbf{I}$. The sensitive subset of geometry-related indexes is selected by quantifying two indicators: (1) Pearson correlation coefficient (PCC), and (2) Laplacian Score (LS). More specifically, the PCC is a measure of the linear correlations between the indexes and the resulting power levels, and it has a range of $[-1, 1]$. Indexes with the PCC values within $[-1, -0.5]$ and $[0.5, 1]$ are considered as sensitive indexes. LS is a method of evaluating the features based on their locality preserving power (He et al., 2005), and is derived from Laplacian Eigenmaps (Belkin and Niyogi, 2001) and Locality Preserving Projection (He and Niyogi, 2003). Indexes with the LS values less than -0.6 are considered as sensitive indexes. Based on the results from the calculation of PCC and LS, the joint sector of these two vectors is defined as the sensitive vector **P** in this work.

2.3. Principal component analysis

To extract features from the selected geometry-related indexes **I** for predicting the energy consumption, the PCA methodology is adopted in this work. As one of the most widely used techniques for reducing the dimensionality of the training data, using PCA can increase the interpretability of the results and at the same time minimize the information loss (Jolliffe and Cadima, 2016). By solving an eigenvalue and corresponding eigenvector problem, new uncorrelated variables with maximum variances are generated and they are referred to as principal components. By using PCA, the selected geometry-related indexes **I** can be transformed into a new coordinate space. In this new coordinate space, the projection of the geometry-related indexes with the greatest variance lies on the first coordinate, the projection of the geometry-related indexes with the second greatest variance lies on the second coordinate, and so on. These coordinates are also referred to as principal components.

In this work, the PCA is performed by (1) the normalization of each attributes in **I**, and (2) the factorization of the matrix using the singular value decomposition (SVD) method. Note that, benefited from eliminated effects of various measurement units, the normalized geometry-related indexes are used in the factorization step to extract geometry features. SVD is the factorization of a real

or complex matrix by generating the eigen-decomposition of a positive semidefinite normal matrix to any dimensional matrix via a polar decomposition. The projection in the new coordinate space **T** obtained using SVD can be written as follows.

$$\mathbf{T} = \mathbf{IW} = \mathbf{U\Sigma W^T W} = \mathbf{U\Sigma} \tag{1}$$

In this equation, **U** denotes the left singular vectors of index vector **I**, **Σ** represents the rectangular diagonal matrix of square root of the eigenvalues of $\mathbf{I^T I}$ as singular values, and **W** stands for the right singular vectors of **I**.

With each eigen value of $\mathbf{I^T I}$ proportional to the portion of the variance that associated with the corresponding eigen vector, singular value as the square root of the eigenvalues indicate the portion of the variance that associated with eigen vector as well. Based on the singular values, the critical principal components can be selected and used for fitting the regression model. The space made by the first *c* critical principal components can be written as follows.

$$\mathbf{T_c} = \mathbf{U_c \Sigma_c} = \mathbf{PW_c} \tag{2}$$

In this equation, $\mathbf{W_c}$ represents the right singular vectors who own the first *c* largest singular value.

2.4. Power consumption prediction models

To obtain the most effective models in terms of predicting the power consumption, three different types of models are considered in this work, i.e., stepwise linear regression model, regular back-propagation model (shallow neural network), and stack autoencoders (deep learning-based model). Note that by using SAE, features are extracted automatically, and prediction is performed through self-learning process; while in linear regression model and neural network, the features are selected or extracted by sensitivity analysis and PCA.

SAE as a popular used deep learning-based method was adopted for automatic feature extraction other than manually selected as PCA. As a quickly rising technique, deep learning techniques has been validated effectively on extracting features by digging nonlinear complicated relationship between the explanatory variables and target response in various areas, such as image recognition (Russakovsky et al., 2015), speech recognition (Dahl et al., 2012), financial market predictions (Fischer and Krauss, 2018).

3. Results and analysis

In this section, feature selection and extraction results are presented. In addition, three different prediction models are obtained using selected and extracted features, and their performance is compared.

3.1. Sensitivity analysis for feature selection

The selected geometry-related indexes can be formulated as follows.

$$\mathbf{I} = \{BS, PS, \alpha, \delta, N_l, Mean,\ Mode, Max, Min, R, Var, STD, IR, ID\} \tag{3}$$

The vector **I** contains fourteen different attributes, i.e., the bounding surface area *BS*, the printing surface area *PS*, the ratio of printing surface area and bounding area α, the ratio of hollow area and printing surface area δ, the number of printing full looped shape N_l, the average value of printing shape curvature *Mean*, the mode of printing shape curvature *Mode*, the maximum value of printing shape curvature *Max*, the minimum value of printing shape curvature *Min*, the range of printing shape curvature *R*, the variance of printing shape curvature *V*, the standard deviation of printing shape curvature *STD*, the interquartile range of printing shape curvature *IR*, and the index of a certain layer *ID*. As an example, a sliced layer with cross section information is shown in Fig. 4.

The quantification of PCC leads to the sensitive indexes as follows.

$$\mathbf{P_{PCC}} = \{ID, IR, PS, BS, \alpha, Mode, N_l\} \tag{4}$$

Note that the indexes in vector $\mathbf{P_{PCC}}$ are sorted in descending order based on the values of PCC. In addition, the sensitive indexes selected by LS values are shown as follows.

$$\mathbf{P_{LC}} = \{BS, PS, N_l, Mean, STD, R, IR\} \tag{5}$$

The indexes in vector $\mathbf{P_{LC}}$ are sorted in descending order according the values of LS. The results of PCC and LS are illustrated in Fig. 5.

Based on $\mathbf{P_{PCC}}$ and $\mathbf{P_{LC}}$, the sensitive set of indexes can be formulated as follows.

$$\mathbf{P} = \{BS, PS, N_l, IR\} \tag{6}$$

3.2. Principal component analysis for feature extraction

To reduce the data redundancy and improve the data integrity, the geometry-related indexes in vector **I** are first normalized. The normalization and PCA with the normalized vector can be formulated as follows.

$$\mathbf{I_N} = \frac{\mathbf{I} - Mean(\mathbf{I})}{STD(\mathbf{I})} \tag{7}$$

$$\mathbf{T_N} = \mathbf{I_N W_N} = \mathbf{U_N \Sigma_N W_N}^{\mathbf{T}} \mathbf{W_N} = \mathbf{U_N \Sigma_N} \tag{8}$$

The normalized vector $\mathbf{I_N}$ is used in PCA, in which 14 principal components are generated from the normalized indexes. The explained variances and accumulative explained variances of these 14 principal components are illustrated in Fig. 6. It should be noted

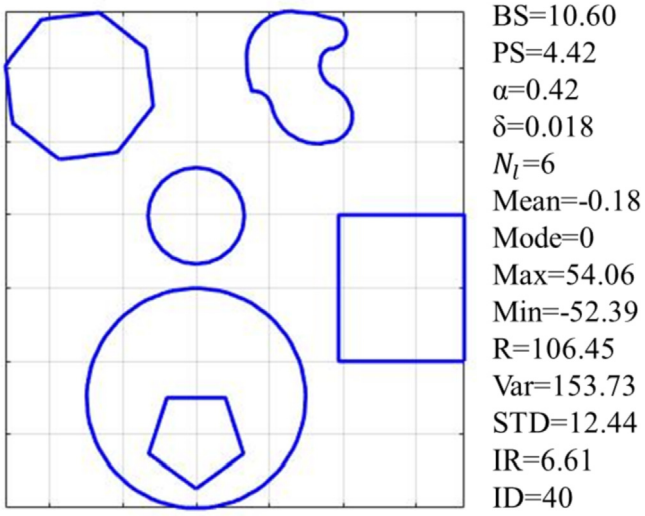

Fig. 4. An example of the index values of a cross section layer.

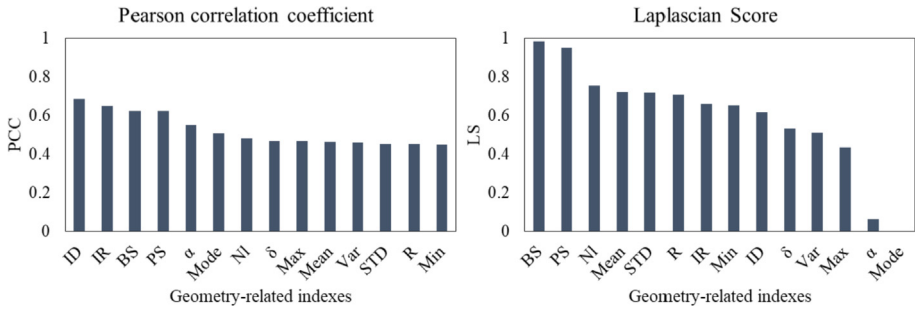

Fig. 5. The results of Pearson correlation coefficient and Laplacian Score.

that these 14 principal components have been sorted in descending order according to their explained variances. As demonstrated in the figure, the first 8 components have the accumulative explained variances as 98.50%, which indicates that these 8 principal components can sufficiently represent the normalized index space. Therefore, the first 8 principal components are selected as critical principal components in vector $\mathbf{T_c}$.

To demonstrate the capability of these principal components in terms of estimating the power levels, a series of plots are obtained and shown in Fig. 7. These scatter plots indicate that the obtained critical components have the capability of affecting the power consumption.

3.3. Model performance comparison

The selected features based on the sensitivity analysis **P** and the extracted features based on PCA $\mathbf{T_c}$ are both used for fitting different types of models. The model performance in terms of the values of Root-mean-square error (RMSE) and Mean squared error (MSE) is illustrated in Table 1. It can be observed from the table that the neural network model using predictor $\mathbf{T_c}$ has the lowest value of averaged RMSE, which is the mean RMSE of both training and testing. This indicates that the neural network model using critical components $\mathbf{T_c}$ as features has the best overall performance. The deep learning-based mode, on the other hand, also has low averaged RMSE and the lowest RMSE value for the testing performance. This shows that in a deeper structure, more effective features can be extracted through self-learning considering their performance in terms of model testing.

The averaged RMSE value is the highest in the linear regression model using sensitive predictor **P**, which indicates the relatively poor performance compared to other models. This is possibly because over-simplified linear relationships are assumed between input information and output. In addition, as illustrated in Table 1, the neural network model using predictor $\mathbf{T_c}$ from PCA has lower MSE and RMSE in both training and testing, compared to the model using predictor **P** from sensitivity analysis. The structures of these two backpropagation neural network models are shown in Fig. 8. Note that the training and testing divisions for these two models are randomly selected, and the training algorithm used is Levenberg-Marquardt.

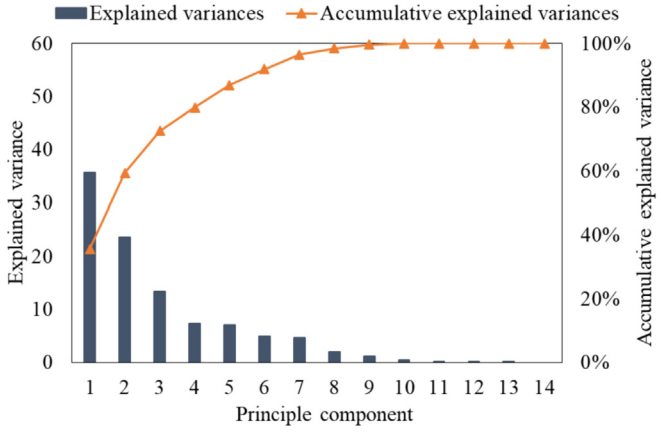

Fig. 6. The pareto chart for variances principal components.

According to the model structures, it can be observed that the neural network model obtained from extracted predictors from PCA $\mathbf{T_c}$ has three hidden layers while the model from sensitive predictors **P** has two hidden layers. In general, more hidden layers usually lead to better model training performance, but sometimes excessive number of hidden layers can cause overfitted testing performance. To further investigate the training performance of these two shallow neural networks using **P** and $\mathbf{T_c}$, the MSE results and training statistics are shown in in Fig. 9 and Fig. 10, respectively.

As can be observed from Figs. 9 and 10, the number of iterations before convergence in the shallow neural network using sensitive predictor **P** is significantly less than that in the shallow neural network using critical components $\mathbf{T_c}$. This indicates the higher training efficiency of using sensitive predictor **P**. However, the MSE value of the neural network model using **P** is slightly higher than using $\mathbf{T_c}$, which shows that although the neural network using critical components $\mathbf{T_c}$ requires more iterations before convergence, it can estimate the power consumption with less errors in the training stage.

In addition, the regression results of both shallow neural networks are demonstrated in Fig. 11. A higher R square value (0.72935) can be observed in the regression results obtained by using predictor $\mathbf{T_c}$ than predictor **P** (0.46529), indicating stronger relation between predictor $\mathbf{T_c}$ and power consumption than predictor **P** and power consumption. Therefore, predictor $\mathbf{T_c}$ outperform the predictor **P** for power consumption with both linear and nonlinear models.

As also illustrated in Table 1, SAE outperformed shallow neural network models with a lower testing RMSE and less overfitting occurrences because of the least difference between the RMSE of training and testing. The structure of obtained deep learning-based model is demonstrated in Fig. 12. The SAE is consisted of one input layer, two hidden layers and one output layer. In other words, the input information is encoded through encoding weight and bias matrixes in two sequential autoencoders to obtain more abstract expression of the original information. The extracted abstract expression is then transferred back to the original input information with slight errors using the trained decoding weight and bias matrixes. In SAE, due to the minimization of the difference between the original information and the reconstructed information, the

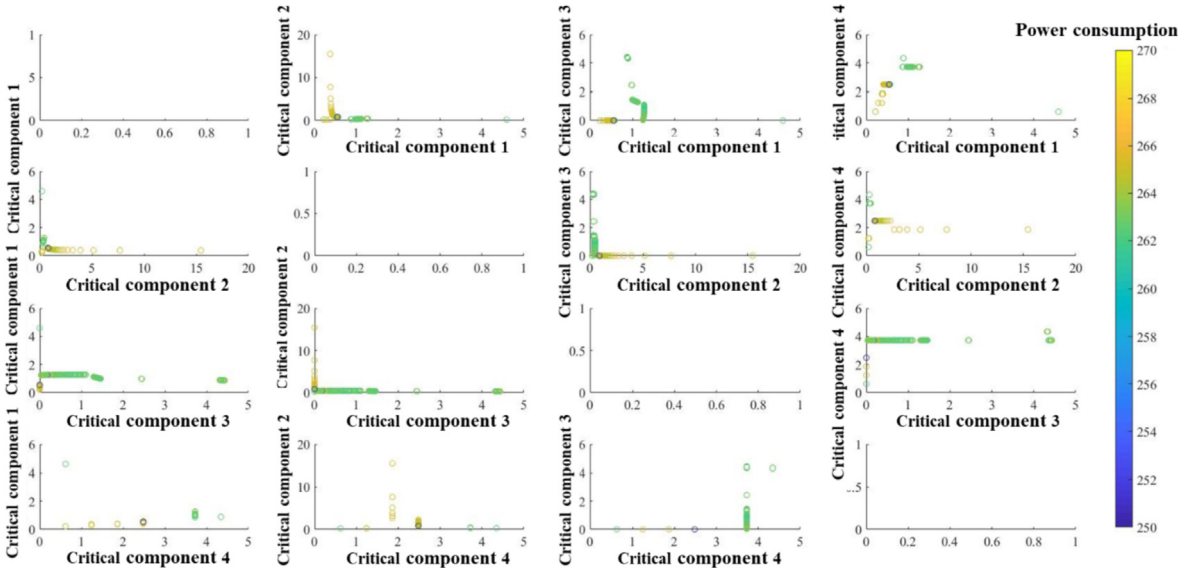

Fig. 7. Predictor projection plots of the first four critical principal components.

Table 1
The model performance comparison.

Model type	Predictor	Averaged RMSE	Training		Testing	
			MSE	RMSE	MSE	RMSE
Linear regression model	**P**	1.58%	6.16E-05	0.79%	5.62E-04	2.37%
	$\mathbf{T_c}$	1.32%	5.96E-05	0.77%	3.46E-04	1.86%
Neural network model	**P**	1.57%	5.89E-05	0.77%	5.56E-04	2.36%
	$\mathbf{T_c}$	0.75%	2.52E-05	0.50%	1.01E-04	1.00%
Deep learning-based model	**I**	0.82%	6.08E-05	0.78%	7.28E-05	0.85%

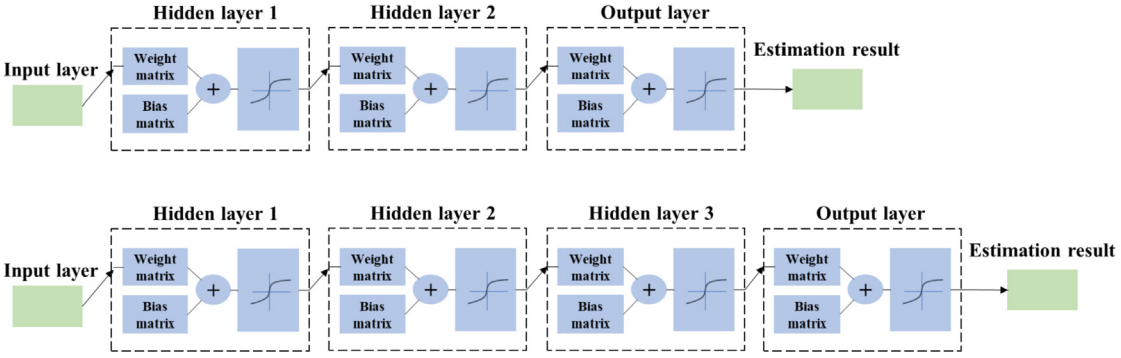

Fig. 8. Structures of neural network models using predictor **P** (upper) and $\mathbf{T_c}$ (lower).

abstract expression extracted at the hidden layer can be used to represent the original information.

The SAE model performance is illustrated in Fig. 13. The best MSE results shown in Fig. 13(a) is 3.4724e-05, which is smaller than that of shallow neural network models. In other words, the automatically extracted features are shown to have better capability in terms of predicting the power consumption. It is observed that the SAE model requires 43 epochs to converge. This indicates that using automatically extracted features via self-learning algorithm, the model can be trained to have higher accuracy and less overfitting occurrences. Additionally, in Fig. 13(b), three training statistics are presented, i.e., Gradient, Mu, and Validation Failure. The main reasons for considering these three training statistics are that the neural network training stops at any of these conditions: (1) the value of Gradient is converged; (2) the value of Mu is higher than the maximum tolerances; and (3) the model reaches the maximum validation failure times. As illustrated in the figure, using the reduced damp factor Mu, the value of backpropagation gradient on each epoch in logarithmic scale is converged in the neural network with small value of MSE. It can also be observed that the model training stops when it reaches the predetermined maximum validation checks as 6. According to the MSE and regression results in Fig. 13(a)(b), it can be concluded that features automatically extracted by SAE through self-learning are more sensitive and effective in predicting the power consumption, compared to features that are manually extracted by PCA or sensitivity analysis.

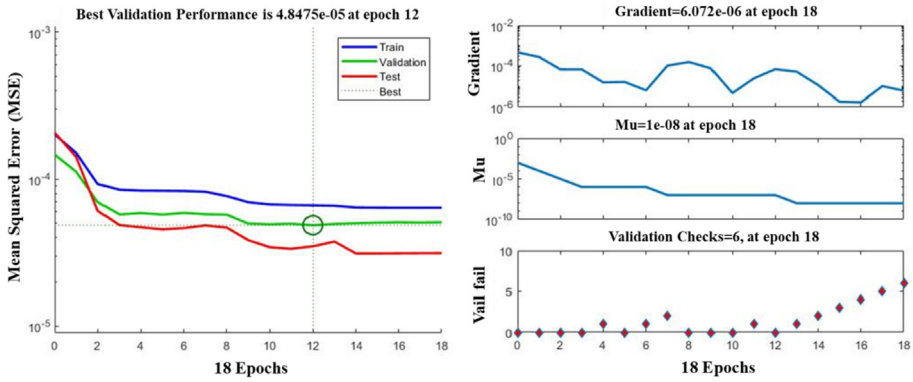

Fig. 9. The training performance of neural network model using predictor.**P**

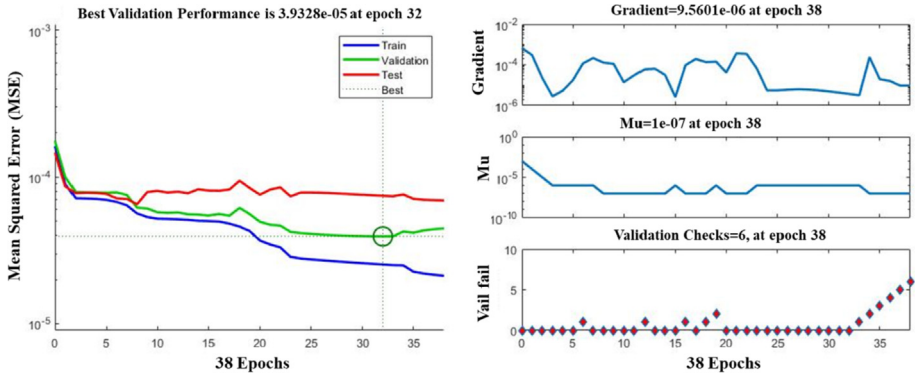

Fig. 10. The training performance of neural network model using predictor.$\mathbf{T_c}$

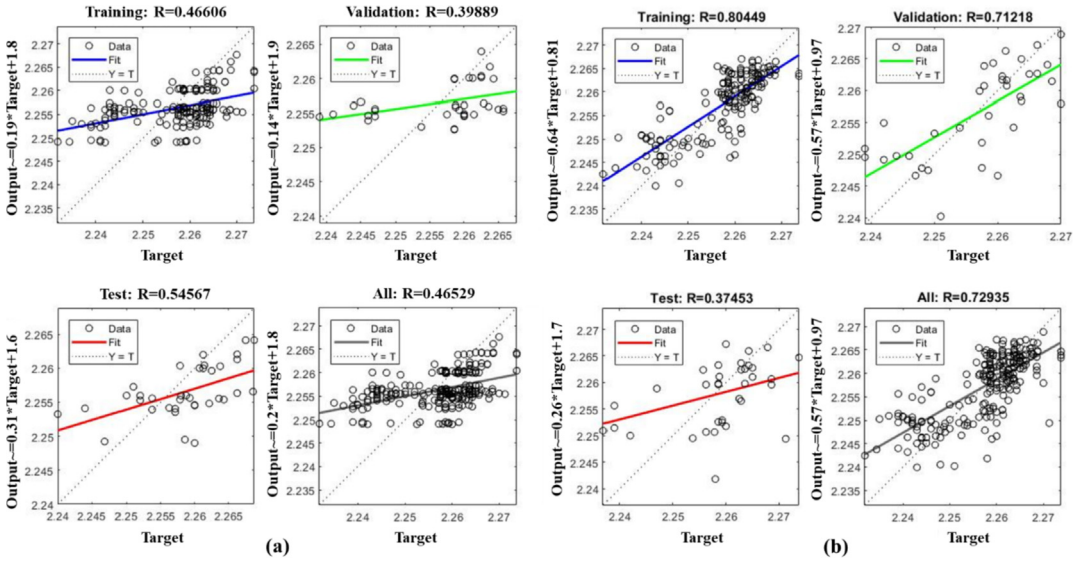

Fig. 11. The regression results of Neural Network models using (a) predictor **P**, and (b) predictor.$\mathbf{T_c}$

Moreover, as shown in Fig. 13(c), the SAE based on automatic extracted features has R-square values of 0.88675, 0.7501, 0.53106, and 0.81444 for training, validation, testing, and overall cases, respectively. This indicates that the SAE structure outperforms the shallow neural network with sensitive indexes considering the testing performance since SAE has slightly greater R-square values compared to the shallow neural network based on PCA extracted features. In SAE, the hard constraint on each sequential autoencoders aims to minimize the difference between the original information and reconstruction, and forces the autoencoders to extract more representative abstract expression from the original information. Hence, the SAE can deliver a more accurate prediction on the power consumption than regular neural network with manually selected/extracted features.

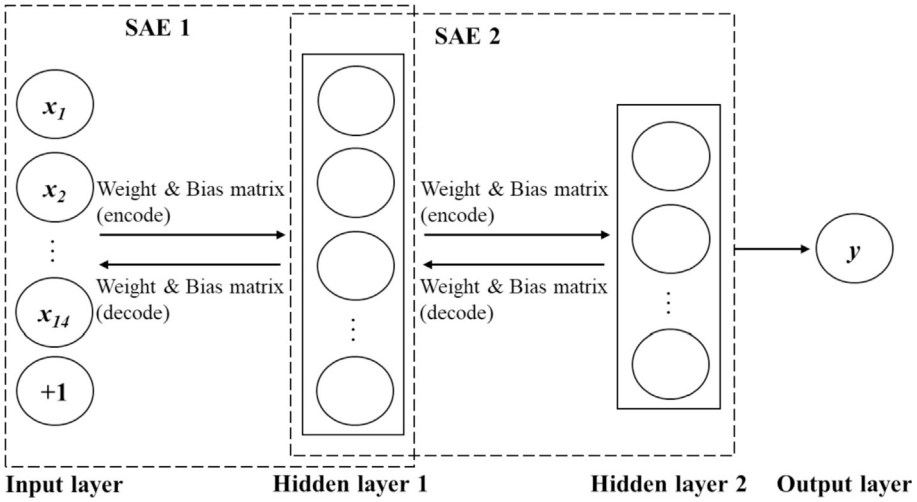

Fig. 12. Structure of deep learning-based model.

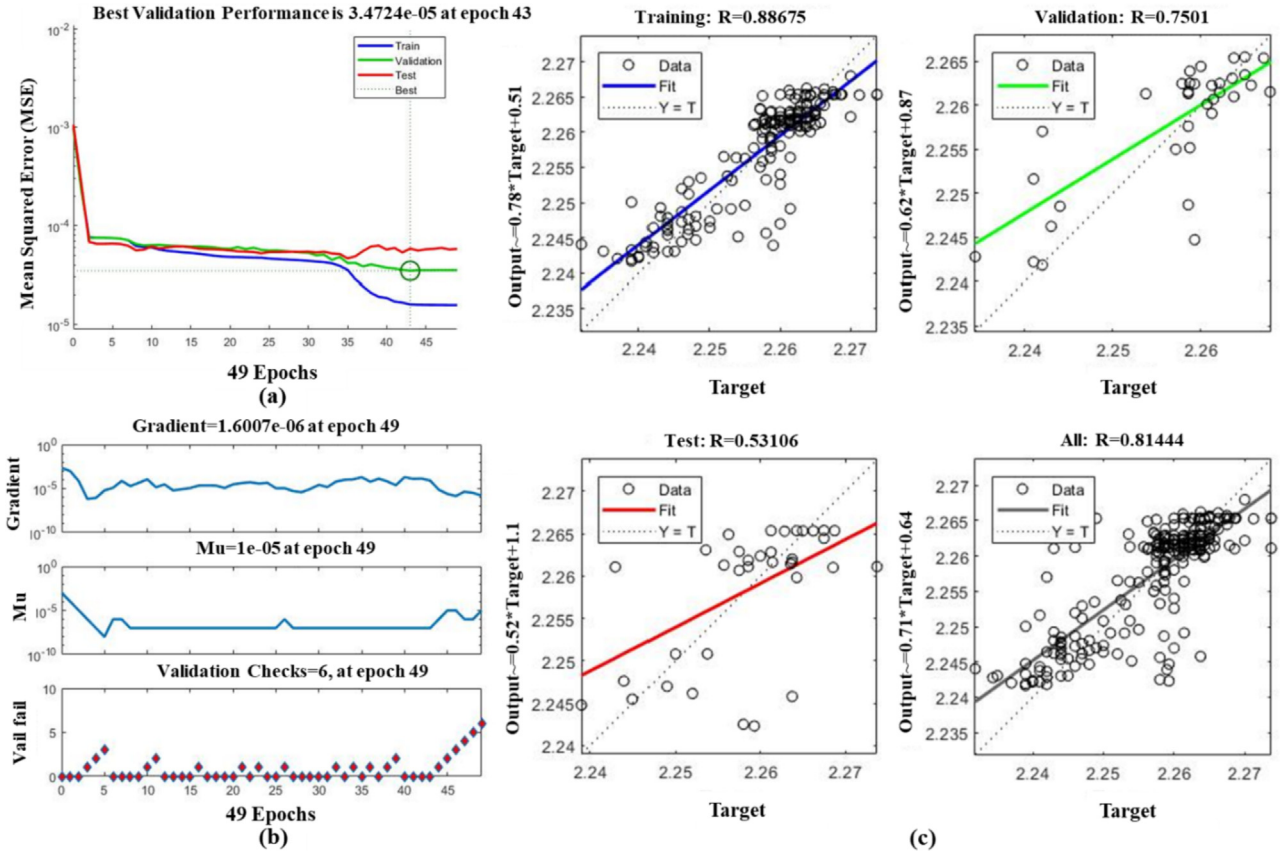

Fig. 13. The training performance and regression results of SAE model.

To further demonstrate the efficiency of using automatically extracted features by SAE, the relationships between the averaged outputs from the hidden layer 2 and their corresponding power consumption is visualized in Fig. 14. This obvious monotonically increasing trend that can be observed from the figure demonstrates the capability of the automatically extracted features in terms of effectively estimating the power consumption.

3.4. Discussion

The trained machine learning models can be used by AM designers as a useful tool to estimate and predict the power consumption for fabricating a certain geometry design using mask image projection stereolithography process. In cases when multiple geometry designs can achieve the same functionality, these models can offer AM designers a chance to evaluate the power

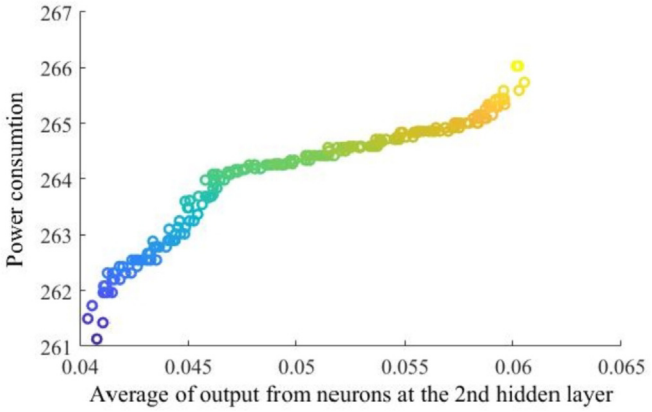

Fig. 14. The visualization of features automatically extracted by stacked autoencoders.

consumption and select a more environmentally friendly design. The results of this work can also aid incorporate the consideration for environmental sustainability into the AM design stage, and open up multidisciplinary collaboration opportunities in related fields. Furthermore, the outcomes of this work will greatly promote the awareness of cleaner production in AM field as well as in manufacturing industry.

4. Conclusion and future work

In this work, machine learning-based approach is used aiming to obtain the appropriate estimation model for the power consumption of MIP SL process. More specifically, three different models are studied (i.e., stepwise linear regression model, shallow neural network model, and stacked autoencoders) while two different feature selection methods are adopted (i.e., sensitivity analysis and PCA). According to the overall model performance comparison, the backpropagation neural network using critical components as predictors has the lowest averaged RMSE of 0.75%, which is around 39.12% lower than other models studied in this work. In addition, the SAE structure has the lowest RMSE 0.85% in terms of testing performance, which is 49.35% lower than the training performance of other investigated models. The deep learning model outperforms the regression model and neural network model at the testing phase, and it will be more applicable in real-life industrial settings.

As an extension of this work, other AM processes will be studied to compare the relationships between geometry characteristics and required power consumption among different AM processes. In addition, other environmental sustainability measures (e.g., material usage and process emissions) will be investigated.

Declaration of competing interest

The authors declare that they have no known competing financial interests or personal relationships that could have appeared to influence the work reported in this paper.

Acknowledgements

The authors truly appreciate the financial support from the U.S. National Science Foundation under Grant Number 1604825.

References

Afshar-Mohajer, N., Wu, C.Y., Ladun, T., Rajon, D.A., Huang, Y., 2015. Characterization of particulate matters and total VOC emissions from a binder jetting 3D printer. Build. Environ. 93, 293–301. https://doi.org/10.1016/j.buildenv.2015.07.013.

ASTM, 2012. Standard terminology for additive manufacturing technologies. F2792-12a i 11–13. https://doi.org/10.1520/F2792-12A.2.

Balogun, V.A., Kirkwood, N., Mativenga, P.T., 2015. Energy-consumption-and-carbon-footprint-analysis-of-Fused-Deposition-Modelling doc 6.

Balogun, V.A., Kirkwood, N.D., Mativenga, P.T., 2014. Direct electrical energy demand in fused deposition modelling. In: Procedia CIRP, pp. 38–43. https://doi.org/10.1016/j.procir.2014.06.029.

Baumers, M., Tuck, C., Bourell, D.L., Sreenivasan, R., Hague, R., 2011. Sustainability of additive manufacturing: measuring the energy consumption of the laser sintering process. Proc. Inst. Mech. Eng. B J. Eng. Manuf. 225, 2228–2239. https://doi.org/10.1177/0954405411406044.

Baumers, M., Tuck, C., Wildman, R., Ashcroft, I., Rosamond, E., Hague, R., 2012. Combined build–time, energy consumption and cost estimation for direct metal laser sintering. Proc. Twenty Third Annu. Int. Solid Free. Fabr. Symp. Addit. Manuf. Conf. 53, 1689–1699. https://doi.org/10.1017/CBO9781107415324.004.

Belkin, M., Niyogi, P., 2001. Laplacian Eigenmaps and spectral techniques for embedding and clustering. NIPS (News Physiol. Sci.) 7, 956–963, 10.1.1.19.9400. https://papers.nips.cc/paper/1961-laplacian-eigenmaps-and-spectral-techniques-for-embedding-and-clustering.pdf.

Choren, J.A., Heinrich, S.M., Silver-Thorn, M.B., 2013. Young's modulus and volume porosity relationships for additive manufacturing applications. J. Mater. Sci. https://doi.org/10.1007/s10853-013-7237-5.

Dahl, G.E., Yu, D., Deng, L., Acero, A., 2012. Context-dependent pre-trained deep neural networks for large-vocabulary speech recognition. IEEE Trans. Audio Speech Lang. Process. 20, 30–42. https://doi.org/10.1109/TASL.2011.2134090.

Dambatta, Y.S., Sarhan, A.A.D., 2016. Surface roughness analysis, modelling and prediction in fused deposition modelling additive manufacturing technology. World Acad. Sci. Eng. Technol. Int. J. Mech. Aerospace, Ind. Mechatron. Manuf. Eng. 10, 1568–1575.

Domingo-Espin, M., Puigoriol-Forcada, J.M., Garcia-Granada, A.A., Llumà, J., Borros, S., Reyes, G., 2015. Mechanical property characterization and simulation of fused deposition modeling Polycarbonate parts. Mater. Des. 83, 670–677. https://doi.org/10.1016/j.matdes.2015.06.074.

Fischer, T., Krauss, C., 2018. Deep learning with long short-term memory networks for financial market predictions. Eur. J. Oper. Res. 270, 654–669. https://doi.org/10.1016/j.ejor.2017.11.054.

He, X., Cai, D., Niyogi, P., 2005. Laplacian Score for feature selection. In: Proc.NIPS, pp. 507–514. http://books.nips.cc/papers/files/nips18/NIPS2005_0149.pdf.

He, X., Niyogi, P., 2003. Locality preserving projections. Adv. Neural Inf. Process. Syst. 16, 153–160, 10.1.1.19.9400. http://papers.nips.cc/paper/2359-locality-preserving-projections.pdf.

Jolliffe, I.T., Cadima, J., 2016. Principal component analysis: a review and recent developments. Phil. Trans. R. Soc. 374, 20150202.

Li, L., Haghighi, A., Yang, Y., 2018a. A novel 6-axis hybrid additive-subtractive manufacturing process: design and case studies. J. Manuf. Process. 33, 150–160. https://doi.org/10.1016/j.jmapro.2018.05.008.

Li, L., Haghighi, A., Yang, Y., 2018b. Theretical modeling and prediction of surface roughness for hybrid additive-subtractive manufacturing processes. IISE Trans. https://doi.org/10.1080/24725854.2018.1458268 (in press).

Lindemann, C., Jahnke, U., Moi, M., Koch, R., 2012. Analyzing product lifecycle costs for a better understanding of cost drivers in additive manufacturing. Int. Solid Free. Fabr. Symp. 23, 177–188. https://doi.org/10.1007/s13398-014-0173-7.2.

Lu, L., Guo, P., Pan, Y., 2017. Magnetic-field-assisted projection stereolithography for three-dimensional printing of smart structures. J. Manuf. Sci. Eng. 139, 071008 https://doi.org/10.1115/1.4035964.

Manyika, J., Chui, M., Bughin, J., Dobbs, R., Bisson, P., Marrs, 2013. Disruptive Technologies: Advances that Will Transform Life, Business, and the Global Economy, vol. 163. McKinsey Glob. Insitute.

Meteyer, S., Xu, X., Perry, N., Zhao, Y.F., 2014. Energy and material flow analysis of binder-jetting additive manufacturing processes. In: Procedia CIRP, pp. 19–25. https://doi.org/10.1016/j.procir.2014.06.030.

Mognol, P., Lepicart, D., Perry, N., 2006. Rapid prototyping: energy and environment in the spotlight. Rapid Prototyp. J. 12, 26–34. https://doi.org/10.1108/13552540610637246.

Paul, R., Anand, S., 2012. Process energy analysis and optimization in selective laser sintering. J. Manuf. Syst. 31, 429–437. https://doi.org/10.1016/j.jmsy.2012.07.004.

Russakovsky, O., Deng, J., Su, H., Krause, J., Satheesh, S., Ma, S., Huang, Z., Karpathy, A., Khosla, A., Bernstein, M., Berg, A.C., Fei-Fei, L., 2015. ImageNet large scale visual recognition challenge. Int. J. Comput. Vis. 115, 211–252. https://doi.org/10.1007/s11263-015-0816-y.

Sreenivasan, R., Bourell, D.L., 2009. Sustainability study in selective laser sintering – an energy perspective. Solid Free. Fabr. Symp. 257–265.

Telenko, C., Conner Seepersad, C., 2012. A comparison of the energy efficiency of selective laser sintering and injection molding of nylon parts. Rapid Prototyp. J. 18, 472–481. https://doi.org/10.1108/13552541211272018.

Telenko, C., Seepersad, C.C., 2010. A comparative evaluation of energy consumption of selective laser sintering and injection molding of nylon parts. Solid free. Fabr. Symp. 41–54.

Timothy, S., Giovanny, A., Fu, Z., 2017. Characterization of particle emission from fuse deposition modeling printers. In: ASME 2017 12th International Manufacturing Science and Engineering Conference. V002T01A040-V002T01A040.

Verma, a, Rai, R., 2013. Energy efficient modeling and optimization of additive manufacturing processes. 24th Int. SFF Symp. - An Addit. Manuf. Conf. SFF 231–241, 2013.

Wohlers Report, vol. 2018, 2018. Wohlers Associates.

Xu, X., Meteyer, S., Perry, N., Zhao, Y.F., 2015. Energy consumption model of Binder-jetting additive manufacturing processes. Int. J. Prod. Res. 53, 7005–7015. https://doi.org/10.1080/00207543.2014.937013.

Yang, Y., Li, L., 2018a. Cost modeling and analysis for mask image projection stereolithography additive manufacturing: simultaneous production with mixed geometries. Int. J. Prod. Econ. https://doi.org/10.1016/j.ijpe.2018.09.023.

Yang, Y., Li, L., 2018b. Total volatile organic compound emission evaluation and control for stereolithography additive manufacturing process. J. Clean. Prod. 170, 1268–1278. https://doi.org/10.1016/j.jclepro.2017.09.193.

Yang, Y., Li, L., Pan, Y., Sun, Z., 2017. Energy consumption modeling of stereolithography-based additive manufacturing toward environmental sustainability. J. Ind. Ecol. https://doi.org/10.1111/jiec.12589.

Yang, Y., Li, L., Zhao, J., 2019. Mechanical property modeling of photosensitive liquid resin in stereolithography additive manufacturing: bridging degree of cure with tensile strength and hardness. Mater. Des. 162, 418–428.